Institute of Paper Science and Technology
Atlanta, Georgia

IPST Technical Paper Series Number 954

Concentric Mixing of Hardwood Pulp and Water

A. Giorges, D. White, and T. Heindel

November 2002

Submitted to
TAPPI 2003 Spring Technical Conference
& Trade Fair
May 11-15, 2003
Chicago, Illinois

INSTITUTE OF PAPER SCIENCE AND TECHNOLOGY
PURPOSE AND MISSIONS

The Institute of Paper Science and Technology is an independent graduate school, research organization, and information center for science and technology mainly concerned with manufacture and uses of pulp, paper, paperboard, and other forest products and byproducts. Established in 1929 as The Institute of Paper Chemistry, the Institute provides research and information services to the wood, fiber, and allied industries in a unique partnership between education and business. The Institute is supported by 41 member companies. The purpose of the Institute is fulfilled through four missions, which are:

- to provide a multidisciplinary graduate education to students who advance the science and technology of the industry and who rise into leadership positions within the industry;
- to conduct and foster research that creates knowledge to satisfy the technological needs of the industry;
- to provide the information, expertise, and interactive learning that enable customers to improve job knowledge and business performance;
- to aggressively seek out technological opportunities and facilitate the transfer and implementation of those technologies in collaboration with industry partners.

ACCREDITATION

The Institute of Paper Science and Technology is accredited by the Commission on Colleges of the Southern Association of Colleges and Schools (1866 Southern Lane, Decatur, Georgia 30033-4097: Telephone number 404-679-4501) to award the master of science and doctor of philosophy degrees.

NOTICE AND DISCLAIMER

The Institute of Paper Science and Technology (IPST) has provided a high standard of professional service and has put forth its best efforts within the time and funds available for this project. The information and conclusions are advisory and are intended only for internal use by any company who may receive this report. Each company must decide for itself the best approach to solving any problems it may have and how, or whether, this reported information should be considered in its approach.

IPST does not recommend particular products, procedures, materials, or service. These are included only in the interest of completeness within a laboratory context and budgetary constraint. Actual products, materials, and services used may differ and are peculiar to the operations of each company.

In no event shall IPST or its employees and agents have any obligation or liability for damages including, but not limited to, consequential damages arising out of or in connection with any company's use of or inability to use the reported information. IPST provides no warranty or guaranty of results.

CONCENTRIC MIXING OF HARDWOOD PULP AND WATER

Aklilu T. G. Giorges*, **David E. White***†, and **Theodore J. Heindel****
*Institute of Paper Science and Technology, Atlanta, Georgia 30318
** Iowa State University, Ames, Iowa 50011

ABSTRACT

Concentric mixing experiments with velocity ratios of up to 6 have been completed using hardwood pulp of 1.0, 1.9, and 2.9% consistency and water. Qualitative observations reveal that by increasing the velocity ratio, the inner jet spread angle is found to be larger (i.e., the jet spreads faster) and the downstream mixing region is more uniform. Furthermore, local consistency measurements show a flattening of the concentration profile with increasing velocity ratio, confirming mixing improves as velocity ratio increases.

The mixing of hardwood pulp fiber with water is different from water-water mixing when the velocity ratio R_v (ratio of inner:outer velocity) is small. For the fiber stock tested, the mixing is found to be significantly dependent on the stock consistency when the velocity ratio is small ($R_v \cong 1$). This result indicates that shear stress and turbulence required to fully dislodge the fiber network are not delivered by the fluid streams when the velocity ratio is small. Thus, mixing is due to hydrodynamic instabilities and macroscale variations, which leads to downstream nonuniformities.

When the velocity ratio is high, the mixing efficiency is found to be more strongly dictated by the velocity ratio than the consistency. This is evidence that once the fiber network strength is overcome by shear stress and turbulence, the mixture behaves as a conventional Newtonian fluid in turbulent flow. The mixing at high velocity ratio is due to microscale turbulence that leads to a relatively uniform downstream mixture. In addition, when the flow is turbulent, the mixing process is not affected significantly by the stock consistency.

Turbulent hardwood pulp and water concentric mixing is modeled with the standard k-ε turbulence model. Numerical studies show that the closure constants in the turbulence model can influence the predicted mixing effects. Constant values of $C_{1\varepsilon} = 1.88$ and $C_{2\varepsilon} = 2.4$ for the standard k-ε model are used to obtain reasonable qualitative agreement with the experimental data when the velocity ratio is high.

INTRODUCTION

The concentric mixing process appears to be simple, but complex flow phenomena are required to thoroughly mix the two fluid streams. When the two fluid streams enter the mixing region at different velocities, a high shear region forms at the interface between the two fluid streams. Instabilities at this interface cause vortex pairing, intertwining, and rollup. As the vortices evolve downstream, the annular stream cascades toward the center while the center jet disintegrates radially, enabling mixing. Depending on the mixer and mixing fluid behavior, the two streams may or may not mix completely or uniformly.

The degree of mixing in a concentric mixer can depend on the following [1]: the ratio of inner-to-outer pipe diameter; the ratio of inner-to-outer pipe flow rate or velocity; the ratio of specific gravity between the two fluid streams; the inner and outer pipe Reynolds numbers; the pipe surface roughness; and any secondary pipe flows. When one of the constituents is a fiber suspension, additional parameters related to the fiber characteristics (e.g., fiber length, coarseness, flexibility, etc.) also affect the mixing process [2-6]. The process is further complicated due to the tendency of fiber flocculation.

The mixing of a relatively thick fiber stream with a dilute fiber stream or white water is common in the pulp and paper industry. Concentric mixing occurs both in chemical mixing and in the approach flow area immediately ahead of the fan pump, where thick stock is mixed with thin stock to dilute the fiber suspension to the proper headbox consistency. Thick stock is supplied through a basis weight valve and supplies the inner pipe in a pipe-within-a-pipe design. The outer pipe can be supplied with clear accepts, secondary and tertiary screen accepts, deaeration overflow, etc. [7]. This mixing, if not done properly, can significantly affect the spatial and temporal

† Corresponding author: david.white@ipst.edu

consistency and chemical uniformity of the stock leaving the approach flow area, leading to severe MD and CD nonuniformities in the final sheet. TAPPI recently published an approach flow Technical Information Paper which includes guidelines for velocity, differential velocity, and velocity ratio for concentric mixing used for thick stock dilution before the fan pump [7]. However, in view of the importance of thick stock dilution, it was considered that a rigorous analysis of concentric mixing was in order.

When pulp and water streams mix concentrically, there is effective mixing when the shear stress provides enough energy to disrupt the fiber network between the two fluid streams. However, when the shear stress at the interface is less than the shear needed to disrupt the fiber network, the fiber network may not fracture and mix effectively. Introduction of pure water into the mixing chamber does not guarantee good pulp suspension mixing. Effective mixing of the pulp suspension requires the introduction of a continuous shear stress that can overcome the fiber network strength throughout the mixing chamber. In concentric mixers, the shear stress can be managed by varying the flow rate of the streams.

In this study, the concentric mixing process is experimentally investigated using hardwood fiber stock and water streams and velocity ratios in the range $1 \leq R_v \leq 6$. The experimental jet shape is then compared to numerical predictions that were computed using the standard k-ε turbulence model.

EXPERIMENTAL EQUIPMENT AND SETUP

A schematic of a concentric mixing process is shown in Fig. 1. This process involves mixing a fluid from an inner pipe with diameter d, volumetric flow rate q, and mean fluid velocity u, with a fluid in an outer pipe of diameter D, volumetric flow rate Q, and mean fluid velocity v. Typically, the inner pipe fluid (q) is referred to as the "primary fluid", while the outer pipe fluid (Q) is called the "secondary fluid". In many cases, the primary fluid has a specified species concentration C_p while the secondary fluid has a species concentration C_s. One of the important operating parameters in the mixing process is the velocity ratio between the primary (inner) and secondary (outer) fluids (R_v = u/v).

The purpose of the mixing operation is to obtain a uniform species concentration within a short pipe distance from the jet nozzle. As shown in Fig. 1, the jet issuing from the center pipe may be divided into two regions, the potential core region and the entrainment or mixing region. The characteristics of the potential core are identical to those of the primary fluid stream (e.g., u, C_p), while the characteristics of the mixing region vary from those of the primary fluid to those of the secondary fluid.

In this study, we evaluate the concentric mixing performance of a short fiber-water system. The primary fluid is a bleached hardwood pulp suspension at one of three consistencies and is delivered to the mixing region through the center pipe. Water comprises the secondary fluid and is supplied via the outer pipe. Thick stock hardwood pulp of 1.0, 1.9, and 2.9% consistency are studied, at velocity ratios $1 \leq R_v \leq 6$. The fiber characteristics are shown in Table I (Fiber Quality Analyzer, OpTest Equipment, Inc., Hawkesbury, Ontario, Canada). The experimental results are then used to compare and validate the numerically simulated mixing process.

Experimental Equipment

The experimental system is composed of two transparent concentric pipes in the test section, a large mixing tank to hold the primary fluid, a smaller water tank to hold the secondary fluid, a large discharge tank, a pump, and the associated piping, valves, and flow meters (Fig. 2). The test section consists of a transparent inner pipe with inside diameter d = 2.54 cm and a pipe wall thickness of 0.32 cm (Fig. 3). The outer pipe is also transparent and has an inside pipe diameter of D = 6.35 cm. The inner pipe protrudes into the outer pipe approximately λ = 39.4 cm after the 90° bend (Fig. 3). The outer pipe extends approximately L = 58 cm beyond the inner pipe trailing edge before exiting into the discharge tank. Although L = 58 cm, the actual mixing region captured by high-speed video is approximately 25.4 cm downstream of the inner pipe trailing edge, corresponding to a mixing region of approximately 4D.

To quantitatively study the mixing efficiency, four fluid sampling probes are introduced into the mixing pipe at a distance 3.9D downstream from the nozzle. This sampling system is designed to provide a concentration profile that can be used to study the mixture uniformity of the two streams at the location of the probes. The diameters of the sampling tubes are relatively large compared with the fiber size to avoid clogging, and the sampling tube walls are thin enough to minimize their effect on the flow field. The probes have outside diameters of 18 mm and wall

thicknesses of 1 mm and are located at center and off-center of the main pipe (Fig. 4). They are also identified by a designated number corresponding to (1) r = 22.6 mm, (2) r = 20.2 mm, (3) r = 0, and (4) r = 18.0 mm, where r is the radial distance from the mixer centerline to the centerline of the respective probe. Additionally, high-speed video equipment (Olympus America Motion Analyzer with a frame rate of 1000 frames/sec.) is used to qualitatively assess the mixing process over a mixing region of approximately 4D downstream from the nozzle exit.

Mixing Experiments

The primary fluid, the hardwood fiber stock, is identifiable by the white color due to bleaching. This fiber stock is pumped through the inner pipe, while the outer pipe is supplied with clear city water from the elevated secondary fluid tank. High-speed video images are taken at the test section where the two fluid streams are allowed to interact. In addition to the images, samples are taken using the probes at 3.9D downstream from the nozzle.

During the experiments, the mean secondary fluid (water) velocity is held constant at approximately v = 1.3 m/s, while the mean primary fluid (hardwood pulp) velocity is varied between 1.3 m/s to 7.76 m/s, corresponding to a mean velocity ratio range of $1 < R_v < 6$ (Table II). Pulp consistencies of 0.97, 1.86, and 2.91% are tested to address the effect of fiber concentration.

Experimental Analysis

Using the samples taken by the probes, the concentration distribution in the concentric mixer is determined. The uniformity (homogeneity) of the mixture is characterized by determining the second moment of fiber concentration M for the pipe cross-sectional area. This mixing quantity M $\left(=\sigma^2/\bar{c}^2\right)$ is the square of the variation coefficient and was previously defined by Gray [8] and Maruyama et al. [9] as,

$$M = \frac{1}{A}\int_A \left(\frac{c}{\bar{c}} - 1\right)^2 dA, \tag{1}$$

where A is the cross-sectional area of the main pipe, D is the main pipe diameter, $\bar{c}$ is the mean fiber concentration in the mixer, and c denotes the local fiber concentration in a given sample probe. The mean fiber concentration $\bar{c}$ can be written as:

$$\bar{c} = \frac{q}{q+Q} c_o, \tag{2}$$

where c_o, Q, and q represent the initial jet fiber concentration, the outer pipe volumetric flow rate, and the jet (inner pipe) flow rate, respectively.

The second moment M is used to characterize the mixing quality. In this study, after the computation of the concentration distribution over the main pipe cross section, the second moment of mixing M is approximated by the sum of the squares of the local fiber concentration difference from the mean value, written as follows:

$$M = \frac{\sum_{i=1}^{4} \left(\frac{c_i - \bar{c}}{\bar{c}}\right)^2 a_i}{\sum_{i=1}^{4} a_i}, \tag{3}$$

where a_i and c_i are the area and pulp concentration of each sample, respectively. When the fluid is uniformly mixed, the second moment of mixing approaches zero.

Furthermore, the mixing uniformity range is defined as the normalized difference between the mean and local consistencies, as follows:

$$U = \frac{c - \bar{c}}{\bar{c}} \tag{4}$$

This measure allows quantification of the change in the range of concentration distribution relative to the fiber mean concentration. It characterizes the mixing quality and the degree of difference of the concentration, compared with streams if they were completely and uniformly mixed.

EXPERIMENTAL RESULTS

Figs. 5-7 illustrate typical stop-action images of the mixing process experiments from high-speed video equipment for the three consistencies evaluated. Flow is left to right. The bright region downstream of the inner pipe nozzle is the mixing region. The outer pipe boundary is clearly identifiable, and the inner pipe can be recognized by its tip captured on the left-hand side of the image. The dark "+" mark on the outside of the outer pipe represents a distance of 1D. The total length of the mixing region captured by the images is approximately 4D. The white fluid is the fiber stock, and the mixing process can be visually observed from the dispersion of the pulp that had been introduced in the center jet. The sampling ports at 3.9D are located near the right-most "+" mark.

Effect of Velocity Ratio (R_v)

Fig. 5 illustrates the flow structure of 0.97% consistency hardwood pulp-water concentric mixing when R_v = 1.0, 2.89, and 5.68. As expected, the mixing region increases in the radial direction as the fluids evolve downstream. The actual mixing process can be attributed to flow and geometric factors that promote the interaction between the two fluid streams.

A close visual inspection directly downstream of the trailing edge of the inner pipe in Fig. 5a points to a gradual radial increase in the jet, even though the inner and outer jet mean velocities are nearly identical. This agrees with the flow character reported by Dahm et al. [10] for concentric mixers. Although the center jet wall thickness was very small in their case, they concluded that the boundary layer on both sides of the inner pipe introduced a wake, and the evolution of the wake instability caused the two fluid streams to intertwine at the interface. In the current experimental geometry, boundary layers are present on both sides of the inner pipe, creating a velocity defect. Additionally, the inner pipe has a finite thickness, which results in wake formation at the pipe trailing edge. This wake contributes to the interaction between the two fluid streams.

Furthermore, through inspection of multiple images of the R_v = 1.0 mixing process, large vortex rings and weave-like coherent structures are observed along the interface between the two fluids. These structures become unstable as the fluid moves downstream. Reviewing the high-speed video images in slow motion clearly reveals these hydrodynamic instabilities as well as large-scale turbulent interactions that propagate downstream. This finding illustrates that when the streams are near isokinetic (i.e., R_v = 1.0), the downstream mixing process is primarily due to large-scale low-intensity interactions. Fig. 6a and Fig. 7a also show similar characteristics.

Fig. 5b and 5c display representative images of the mixing process for R_v = 2.89 and 5.68. As the mean velocity ratio increases, the inner jet spread angle increases and the large vortex rings observed in the isokinetic case are no longer apparent. Similar trends are also observed at higher consistencies with the increase in velocity ratio in Figs. 6 and 7.

The increase in R_v causes the mixing intensity to increase. Figs. 5b, 5c, 6b, 6c, 7b, and 7c display representative images of the mixing process for R_v = 2.89, 5.68, 2.95, 5.56, 3.07, and 5.92 for hardwood fiber consistencies of 1.0, 1.9, and 2.9%, respectively. As the mean velocity ratio increases, the mixing intensity and level of entrainment increase and the inner jet spread angle increases. In addition, the inner jet and downstream mixing regions appear milky white and more uniform as the mean velocity ratio increases. This is the result of (i) the increase in center jet flow rate, which in turn increases the local fiber concentration of the mixture (see Eq. (2)); (ii) the increase in center jet flow rate which also increases the flow turbulence, augmenting the mixing; and (iii) the large velocity difference between the inner and outer fluids, which creates the shear region and enhances small-scale turbulent mixing, creating a more uniform mixture.

The improvement in the mixing at higher velocity ratios is quantified using the second moment of mixing (M) and the mixing uniformity range (U). Tables III, IV, and V and Fig. 8 provide a summary of these data. (At the highest consistency run (2.9% in Table V), samples were obtained only at 5.92 velocity ratio due to sampling probe

plugging at lower velocity ratios.) As the mixture becomes more uniform, the difference between the samples and the mean mixture concentration approach zero, as do M and U. Thus, decreases in M and U reflect mixing uniformity improvement. As expected, M and U decrease with increase in R_v, clearly indicating improvement in the mixing process with increase in velocity ratio.

Decrease in both M and U at higher R_v is consistent with qualitative experimental observations. The increase in R_v causes the mixing region to change from snake-like to a uniform milky white cone-like shape. In addition, with the increase in the velocity ratio, the jet spread angle is found to be larger (i.e., the jet spreads faster) and the downstream mixing region is more uniform. Mixing is transformed from a large-scale low-intensity process to a small-scale high-intensity process. Both qualitative and quantitative results reveal that increasing the velocity ratio yields a well-mixed fiber blend.

Effect of Stock Consistency

Figs. 5a, 6a, and 7a display representative images of the near isokinetic case for hardwood fiber consistencies of 0.97, 1.86, and 2.91%, respectively. For each consistency, the weave-like structure at the center becomes unstable with increasing downstream distance from the nozzle. However, at high consistency, the weave-like structure is stabilized by the fiber suspension and network formation, while mixing quality degrades. This is also indicated from the increase in second moment of mixing M and the uniformity range U for the isokinetic data at higher consistency (Tables III and IV). This is a direct indication that the mixing intensity is strongly reduced with the increase in concentration, particularly when the velocities of the streams are approximately equal. This is a result of the increase in fiber network strength with concentration, thus requiring more energy to disrupt the fiber network and mix with the water in the annulus.

At R_v of approximately 3 and 6, there are no clear indications that increasing fiber consistency has a consistent and significant effect in hampering the mixing process (Tables III-V; Fig. 8). This seems to indicate that once the shear stress needed to fracture the fiber network is delivered, the fiber stock mixes in a similar manner regardless of the fiber consistency.

NUMERICAL MODEL

The mixing process is simulated as two turbulent miscible fluids with the same density and viscosity, but with different concentrations. For this model, the governing equations and turbulence model are summarized below. Selected numerical results and comparisons to experiments are also provided.

Governing Equations

The governing equations for conservation of mass, momentum, and concentration for steady, incompressible, turbulent viscous fluid flow with constant fluid properties are:

$$\frac{\partial u_i}{\partial x_i} = 0 \tag{5}$$

$$\rho u_j \frac{\partial u_i}{\partial x_j} = -\frac{\partial p}{\partial x_i} + \frac{\partial}{\partial x_j}\left[(\mu + \mu_t)\left(\frac{\partial u_i}{\partial x_j} + \frac{\partial u_j}{\partial x_i}\right)\right] \tag{6}$$

$$\rho u_j \frac{\partial c}{\partial x_j} = \frac{\partial}{\partial x_j}\left[\left(\frac{\mu}{Sc} + \frac{\mu_t}{\sigma_c}\right)\frac{\partial c}{\partial x_j}\right] \tag{7}$$

All quantities have been time averaged in the above equations, and u_i (i = 1, 2) are the mean local velocity components in the axial and radial directions. Also, ρ is the fluid density, p is the time-averaged pressure, μ is the dynamic viscosity, μ_t is the eddy (turbulent) viscosity, c is the time-averaged local fiber concentration, Sc is the Schmidt number, and σ_c is the turbulent Schmidt number (specified as $\sigma_c = 0.7$ in our calculations).

The governing equations are discretized and solved using FLUENT® computational fluid dynamics (CFD) software. FLUENT® uses a finite volume method to discretize the governing equations [11]. It was selected because it can be used to model the conservation equations of multiple fluid streams [12].

The eddy viscosity (μ_t) is specified through the standard k-ε two-equation turbulence model available in FLUENT© [12], allowing simulation of the turbulent mixing process in this study. The standard k-ε model [13] is widely used due to its robustness, computational economy, and reasonable accuracy for a wide range of engineering problems. The basis of the model is that the eddy viscosity is defined by

$$\mu_t = \rho C_\mu \frac{k^2}{\varepsilon} \tag{8}$$

where C_μ is an empirical constant and k and ε are the turbulent kinetic energy and dissipation rates, respectively. These parameters are determined from the following transport equations

$$\rho u_j \frac{\partial k}{\partial x_j} = \frac{\partial}{\partial x_j}\left[\left(\mu + \frac{\mu_t}{\sigma_k}\right)\frac{\partial k}{\partial x_j}\right] + G_k - \rho\varepsilon \tag{9}$$

$$\rho u_j \frac{\partial \varepsilon}{\partial x_j} = \frac{\partial}{\partial x_j}\left[\left(\mu + \frac{\mu_t}{\sigma_\varepsilon}\right)\frac{\partial \varepsilon}{\partial x_j}\right] + C_{1\varepsilon}\frac{\varepsilon}{k}G_k - C_{2\varepsilon}\rho\frac{\varepsilon^2}{k} \tag{10}$$

where $C_{1\varepsilon}$ and $C_{2\varepsilon}$ are empirical constants, and σ_k and σ_ε are the turbulent Prandtl numbers for k and ε, respectively.

The G_k term represents the production of turbulent kinetic energy and is modeled by [12]

$$G_k = \mu_t S^2 \tag{11}$$

where S is the modulus of the mean rate-of-strain tensor defined by

$$S = \sqrt{2S_{ij}S_{ij}} \tag{12}$$

with the mean strain rate given by

$$S_{ij} = \frac{1}{2}\left(\frac{\partial u_i}{\partial x_j} + \frac{\partial u_j}{\partial x_i}\right) \tag{13}$$

In the standard k-ε model, the following constant values are used as defaults in FLUENT©: $C_\mu = 0.09$, $C_{1\varepsilon} = 1.44$, $C_{2\varepsilon} = 1.92$, $\sigma_k = 1.0$, and $\sigma_\varepsilon = 1.3$. Comments on the applicability of these values will be given below.

NUMERICAL RESULTS

The flow conditions are assumed to be axisymmetric to reduce the computational domain from three dimensions to two dimensions. The actual computation domain (Fig. 9) encompasses a radial distance of 3.175 cm (D/2) and an axial distance of 44.45 cm (7D). Note that the computations encompass a 1D length upstream of the trailing edge of the inner pipe and a 6D length downstream. This region is discretized into a numerical computational grid of 36 X 300 nodes, with a slightly higher node density near the inner pipe trailing edge. Fig. 9 shows the upper half of the concentric mixer, with the primary fluid entering from the lower left region and the secondary fluid entering from the upper left region.

It is well known that turbulence enhances the mixing process. Thus, the turbulence model used to simulate mixing plays a major role in determining realistic predictions. It has also been shown that the values of the standard k-ε model constants, $C_{1\varepsilon}$ and $C_{2\varepsilon}$, affect the relative concentration of the mixing streams [14,15]. Giorges and Heindel [16] showed that as $C_{2\varepsilon}$ increases, the length of the potential core of the inner jet decreases and the jet spread increases. As $C_{1\varepsilon}$ increases, the potential core of the inner jet increases and the jet spread decreases. With this information, all test conditions were numerically simulated and then compared to experimental concentration profiles. The specific $C_{1\varepsilon}$ and $C_{2\varepsilon}$ values were then identified that provide reasonable qualitative agreement between the numerically predicted and experimentally observed concentration profiles.

From the experimental results, we observe that when the velocity ratio is large, the mixing process is not strongly dependent on the concentration of the fiber suspension. In addition, for the isokinetic case, the mixing process is

strongly affected by the concentration. Therefore, universal values of $C_{1\varepsilon}$ and $C_{2\varepsilon}$ are not appropriate for all cases. However, when the flow is turbulent and the velocity ratio is large, $C_{1\varepsilon}$ = 1.88 and $C_{2\varepsilon}$ = 2.4 are found to provide reasonable agreement with all experimental data that satisfy these two constraints.

Based on the Reynolds number alone, the streams are in the fully developed turbulent range. However, Reynolds number is not an appropriate measure of fiber suspension turbulence. A range of pulps and pipe diameters have been investigated to identify when fiber suspensions become turbulent [2,17,18]. Duffy [17] proposed Eq. (14) for the onset of turbulence (also termed the onset of drag reduction) when the flow regime begins to transform from plug flow to transitional flow. At this point, plug flow still exists, while a conventional Newtonian liquid (e.g., water) would already be in fully developed turbulence at the same bulk velocity [17]. Hemstrom et al. [19] suggested an equation for fully developed turbulent flow (onset of significant plug reduction) for an unbeaten, unbleached kraft pulp suspension (Eq. 15).

$$V_w = 1.22\, C^{1.40} \tag{14}$$

$$V_{turb} = 1.8\, C^{1.4} \tag{15}$$

V_w and V_{turb} are the mean velocity (in m/s) at the onset of turbulence and the minimum velocity for fully developed turbulent flow, respectively, and C is the oven-dried consistency in percent. Based on Eqs. (14) and (15) and the consistencies investigated in the current study, velocities are calculated where the pulp suspension is considered turbulent (Table VI).

Under conditions where the thick stock pulp is turbulent, it is determined that a common set of constants $C_{1\varepsilon}$ = 1.88 and $C_{2\varepsilon}$ = 2.4 provide reasonable qualitative agreement of the experimentally observed concentration profiles with the numerical simulations. This is concluded by comparing experimental and numerical concentration profiles at 3.9D for runs where the thick stock velocity exceeds the onset of drag reduction (comparing values in Table I versus Table VI) (Figs 10-14). Under these conditions, it is believed that the shear stress at the interface is strong enough to overcome the fiber network strength. Figs. 10-14 show that there are only small qualitative variations between the results, with the largest variations near the mixer centerline. In Figs. 10-14, the dashed lines represent the numerical values for the local concentrations, while the symbols represent the averaged values (either numerical or experimental) over the specific probe areas as shown in Figure 4.

Figs. 15-19 illustrate a single frame of the experimental results and the corresponding numerical predictions for those conditions that satisfy turbulent fiber suspension flow. From the experimental images, the milky white region at the center indicates the potential core and mixing region. However, the numerically simulated mixing process images show that the darker region indicates the annular fluid (water) while the center lighter region represents the center jet and mixing region between the two extremes. The interface of the two streams cannot be exactly predicted due to the time-averaged and steady state nature of the numerical results. Thus, the vortex ring that can be seen at the interface in the experimental image is not observed in the numerical simulations. In general, both images illustrate the mixing process with downstream distance, and the numerical model predicts the qualitative shape of the mixing region between the pulp and clear water streams when the velocity ratio is high and the streams are turbulent.

CONCLUSIONS

The experimental and numerical concentric mixing results presented here reveal that increasing the velocity ratio increases the mixing effectiveness. When the velocity ratio increases, the turbulence and the shear stress at the interface between the two fluid streams increase, causing the fiber network to break and mix with the water. This is an indication that the mixing efficiency increases with increased velocity ratio. Comparisons of the second moment of mixing, M, and the mixture uniformity range, U, for various velocity ratios, R_v, also show that increasing R_v decreases M and U, demonstrating mixing process improvement. When the velocity ratio is high, the second moment of mixing is a stronger function of R_v than consistency, implying that once the shear stress can disperse the fiber network, the flow behaves as if two turbulent Newtonian fluid streams are mixing. This is believed to be the reason why the numerical simulations are in close agreement with the experimental results when the thick stock velocity exceeds that required for turbulent fiber suspension flow. When the fiber stream is turbulent, the concentric mixing process can be simulated using the standard k-ε model with $C_{1\varepsilon}$ = 1.88 and $C_{2\varepsilon}$ = 2.4. Studies also showed that at a low velocity ratio, mixing is inadequate, even after a significant downstream distance.

ACKNOWLEDGMENT

The authors would like to acknowledge the funding and support of the Member Companies of the Institute of Paper Science and Technology. The authors would also like to thank Adele Garner for her contributions to this work.

REFERENCES

1. Forney, L.J., "Jet Injection for Optimum Pipeline Mixing," *Encyclopedia of Fluid Mechanics Volume 2 - Dynamics of Single-Fluid Flows and Mixing*, N.P. Cheremisinoff, Ed., Gulf Publishing Company, Houston, pp. 660-690 (1986).
2. Duffy, G.G., and Lee, P.F.W., "Drag Reduction in the Turbulent Flow of Wood Pulp Suspensions," *APPITA Journal*, 31(4), pp. 280-286 (1978).
3. Stenuf, T.J., and Unbehend, J.E., "Hydrodynamics of Fiber Suspensions," *Encyclopedia of Fluid Mechanics: Vol. 5 - Slurry Flow Technology*, N.P. Cheremisinoff, Ed., Gulf Publishing Company, Houston, pp. 291-308 (1986).
4. Kerekes, R.J., and Schell, C.J., "Characterization of Fiber Flocculation Regimes by a Crowding Factor," *Journal of Pulp and Paper Science*, 18(1), pp. J32-J38 (1992).
5. Helmer, R.J.N., Covey, G.H., and Lai, L.C.-Y., "Laboratory Study of Co-axial Stock Mixing," *APPITA Journal*, 52(3), pp.197-201 (1999).
6. Norman, B., and Tegengren, A., "Stock Preparation- a Key to Grammage Control, " *Paper Technology*, 31(1), pp. 42-43 (1990).
7. TAPPI TIP0404-54, Headbox Approach Piping Guidelines, 2000.
8. Gray, J.B., "Turbulent Radial Mixing in Pipes," *Mixing: Theory and Practice*, Vol. III, Ch.13. Academic Press, 1986.
9. Maruyama, T., Mizushina, T., and Hayashiguchi, S., "Optimum Jet Mixing in Turbulent Pipe Flow," *Kagaku Kogaku Ronbunshu*. 8(4), pp. 1-16, (1982).
10. Dahm, W.N., Frieler, C.E., and Tryggvason, G., "Vortex Structure and Dynamics in the Near Field of a Coaxial Jet," *Journal of Fluid Mechanics*, 241, pp. 371-402 (1992).
11. Patankar, S.V., *Numerical Heat Transfer and Fluid Flow*, Hemisphere Publishing Corp., New York, 1980.
12. Fluent Incorporated, "FLUENT 5 Users Guide," Lebanon, NH, Fluent, Inc., 1998.
13. Jones, W.P., and Launder, B.E., "The Prediction of Laminarization with a Two-Equation Model of Turbulence," *International Journal of Heat and Mass Transfer*, 15, pp. 310-314 (1972).
14. Monclova, L.A., and Forney, L.J., "Numerical Simulation of a Pipeline Tee Mixer," *Industrial and Engineering Chemistry Research*, 34(4), pp. 1488-1493 (1995).
15. Giorges, A.T., Forney, L.J., and Wang, X., "Numerical Study of Multi-Jet Mixing," *Transactions of the Institute of Chemical Engineers, Part A*, Vol. 79, pp. 515-522 (2001).
16. Giorges, A.T., and Heindel, T., "Concentric Mixing of Two Similar Fluids," AIChE 2000 Annual Meeting, November 12-17, 2000, Los Angeles, CA.
17. Duffy, G.G., "Flow of Medium Consistency Wood Pulp Fiber Suspensions," 47th APPITA Annual General Conference Proceedings, pp. 507-514 (1993).
18. Duffy, G.G., "How to Determine Pipe Friction Loss for the Design of Stock Piping Systems," *Proceedings TAPPI Engineering Conference*, pp. 247 (1979).
19. Hemstrom, G., Moller, K., and Norman, B., "Boundary Layer Studies in Pulp Suspension Flow," *TAPPI Journal*, 59(8), pp. 115-118 (1976).

TABLES

Table I. Hardwood pulp fiber length distribution, curl, kink, and percent fines.

	Sample 1	Sample 2
Mean length		
Arithmetic (mm)	0.48±0.010	0.468±0.010
Length weighted (mm)	0.739	0.730
Weight weighted (mm)	0.926	0.917
Mean curl index		
Arithmetic	0.053±0.002	0.054±0.002
Length weighted	0.056	0.058
Percent fines		
Arithmetic (%)	13.2	13.6
Length weighted (%)	1.98	2.09
Mean kink		
Kink index (1/mm)	1.09	1.09
Total kink angle (°)	17.0	17.3
Kinks per mm (1/mm)	0.63	0.65

Table II: Flow conditions used in the hardwood fiber stock-water concentric mixing experiments, with thick stock consistencies of 0.97, 1.86, and 2.91%.

Consistency	Stream	Volumetric Flow Rate		Mean Velocity	Mean Velocity
		(gal/min)	(lit/min)	(m/s)	Ratio
0.97%	Primary	10.4	39.4	1.29	1.00
	Secondary	50.4	191	1.29	
	Primary	29.9	113	3.72	2.89
	Secondary	50.3	190	1.29	
	Primary	58.5	221	7.28	5.68
	Secondary	50.0	189	1.28	
1.86%	Primary	10.6	40.1	1.32	1.02
	Secondary	50.6	191	1.30	
	Primary	30.5	115	3.80	2.95
	Secondary	50.1	190	1.29	
	Primary	56.4	213	7.02	5.56
	Secondary	49.2	186	1.26	
2.91%	Primary	9.56	36.2	1.19	0.91
	Secondary	50.8	192	1.30	
	Primary	31.5	119	3.92	3.07
	Secondary	49.8	188	1.28	
	Primary	50.2	190	7.64	5.92
	Secondary	50.2	190	1.29	

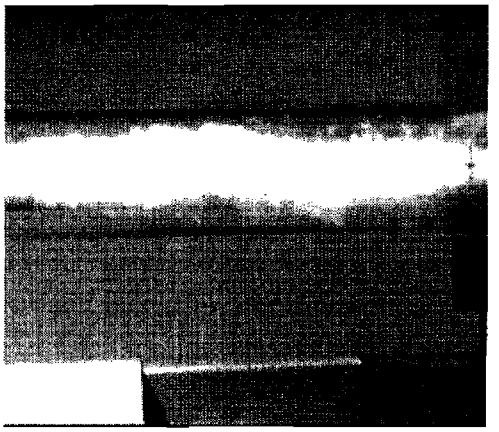

(a)

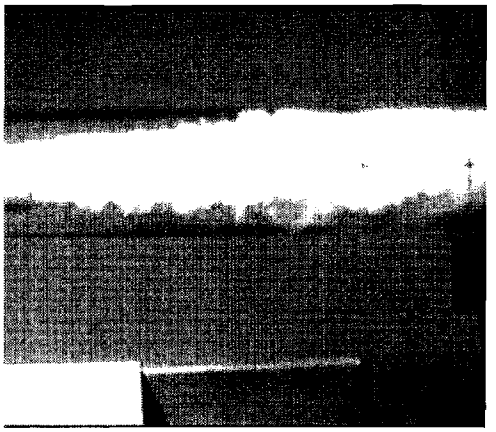

(b)

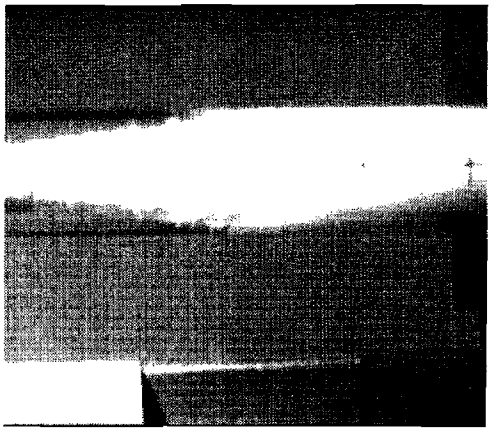

(c)

Figure 7: Images of 2.91% consistency hardwood fiber pulp and water mixing for various velocity ratios (R_v): (a) $R_v = 0.91$, (b) $R_v = 3.07$, and (c) $R_v = 5.92$.

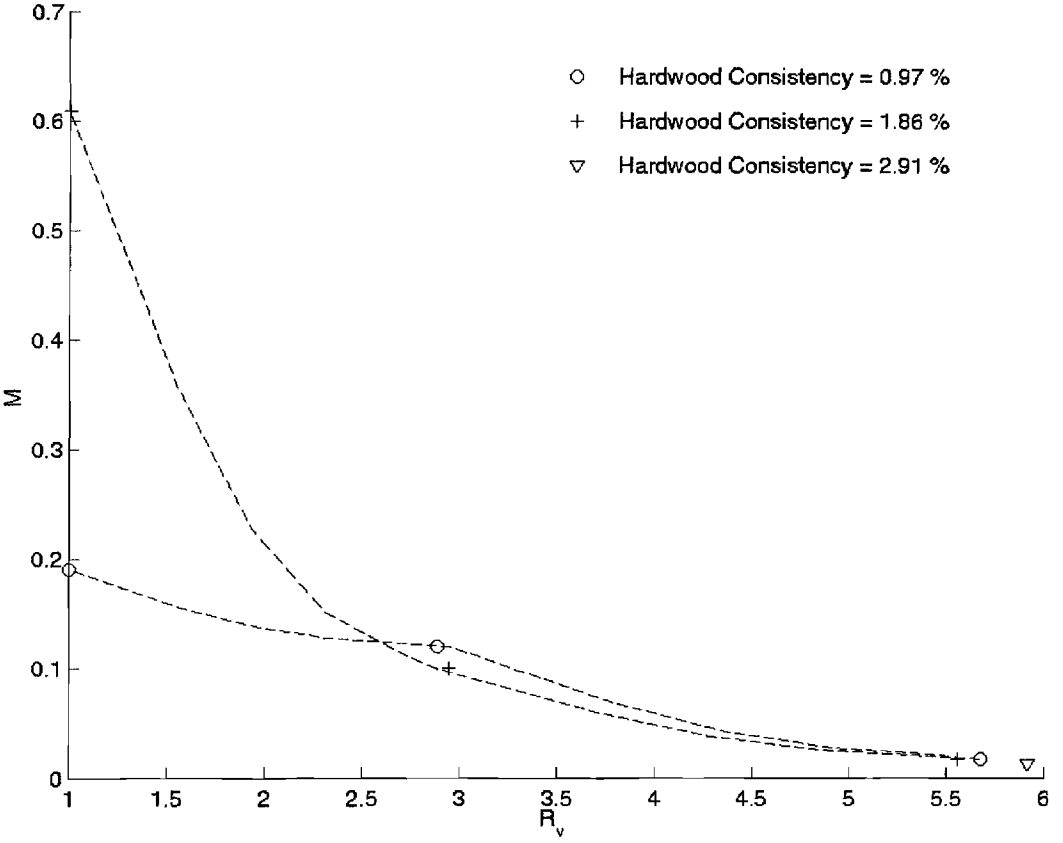

Figure 8: Second moment of mixing (M) vs. velocity ratio (R_v) for 0.97, 1.86, and 2.91% consistency hardwood pulp.

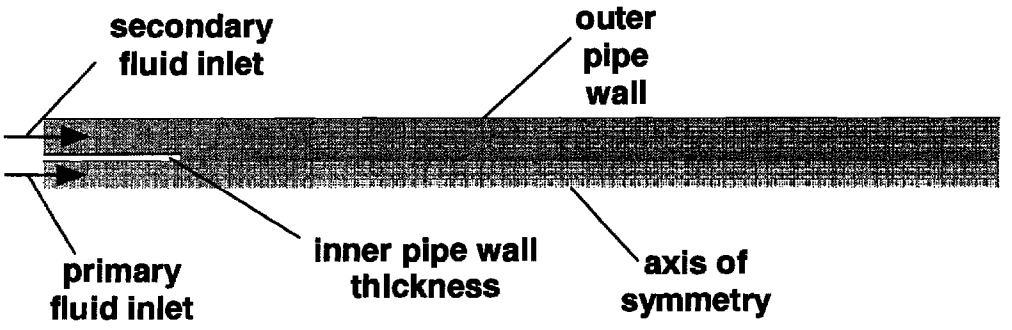

Figure 9: The axisymmetric computation domain.

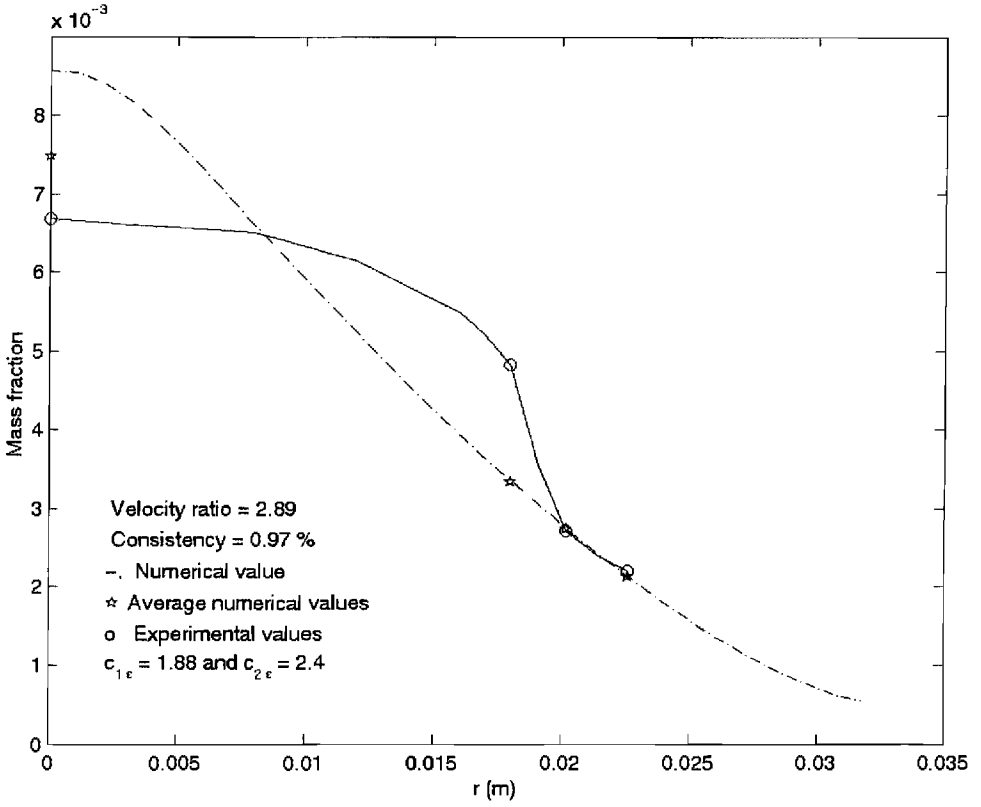

Figure 10: Concentric mixing concentration profile predictions for R_v = 2.89 and 0.97% consistency by the standard k-ε model for $C_{1\varepsilon}$ = 1.88 and $C_{2\varepsilon}$ = 2.4.

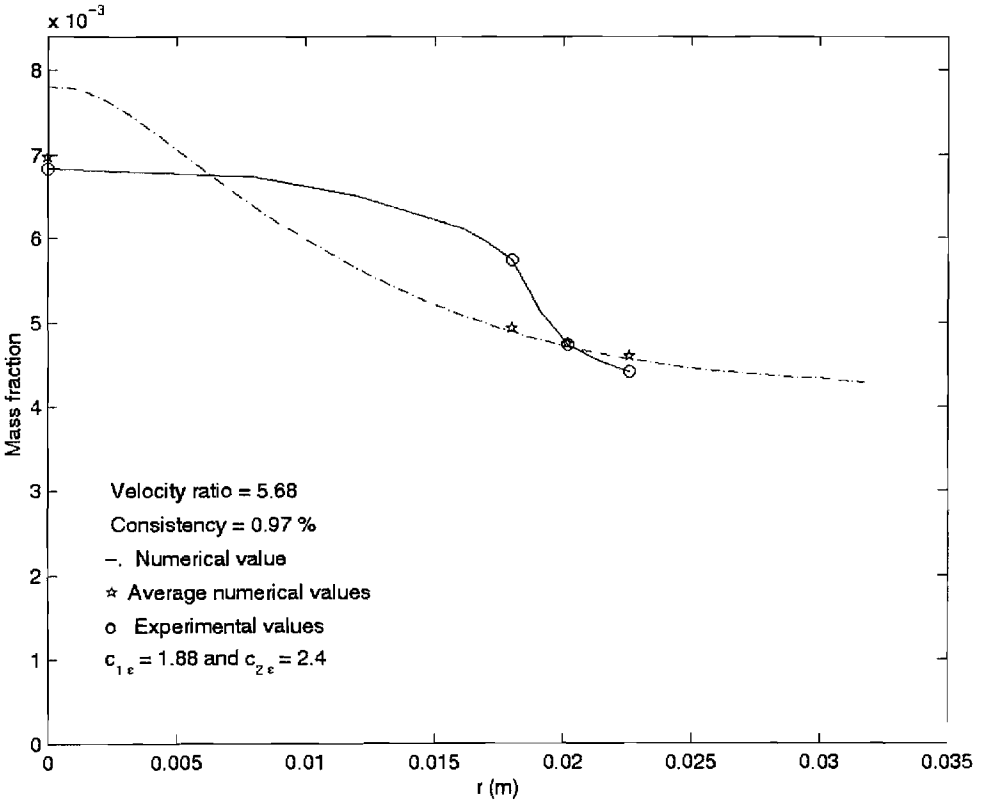

Figure 11: Concentric mixing concentration profile predictions for R_v = 5.68 and 0.97% consistency by the standard k-ε model for $C_{1\varepsilon}$ = 1.88 and $C_{2\varepsilon}$ = 2.4.

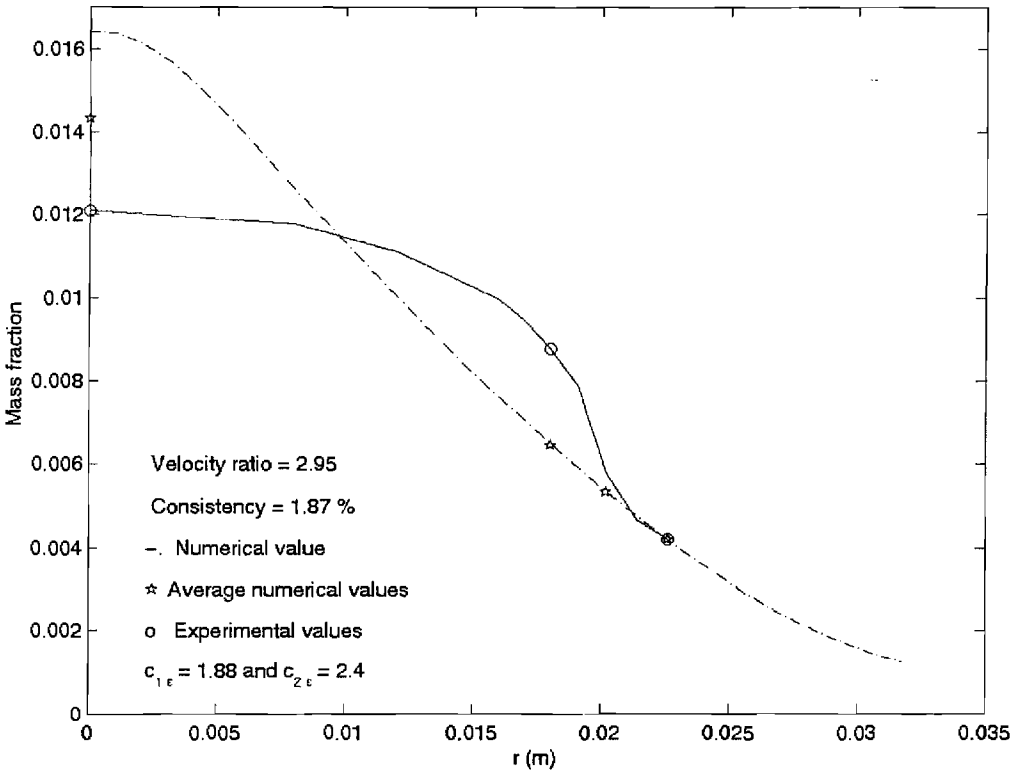

Figure 12: Concentric mixing concentration profile at 3.9D predictions for R_v = 2.95 and 1.86% consistency by the standard k-ε model for $C_{1\varepsilon}$ = 1.88 and $C_{2\varepsilon}$ = 2.4.

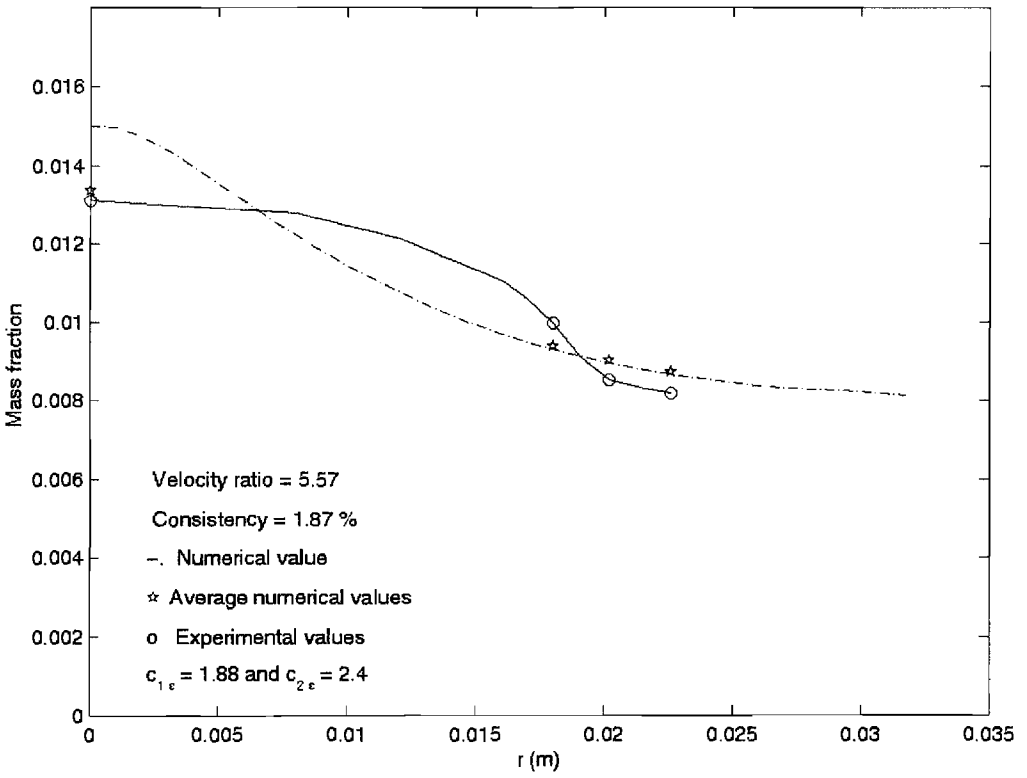

Figure 13: Concentric mixing concentration profile at 3.9D predictions for R_v = 5.57and 1.86% consistency by the standard k-ε model for $C_{1\varepsilon}$ = 1.88 and $C_{2\varepsilon}$ = 2.4.

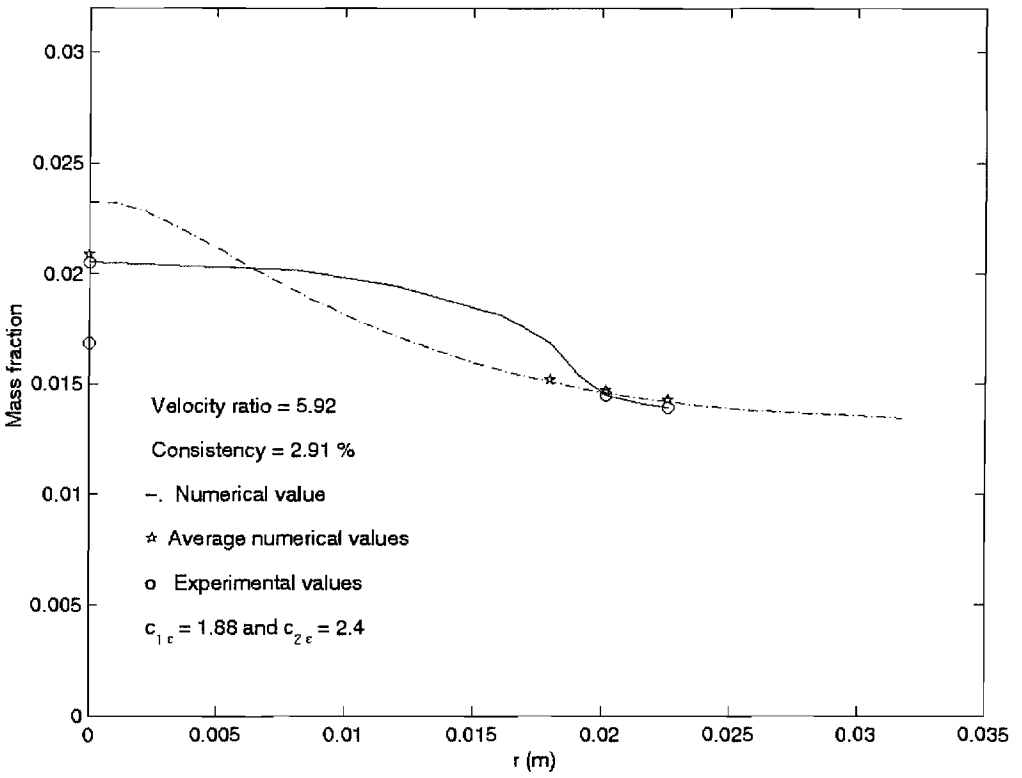

Figure 14: Concentric mixing concentration profile at 3.9D predictions for R_v = 5.92 and 2.91% consistency by the standard k-ε model for $C_{1\varepsilon}$ = 1.88 and $C_{2\varepsilon}$ = 2.4.

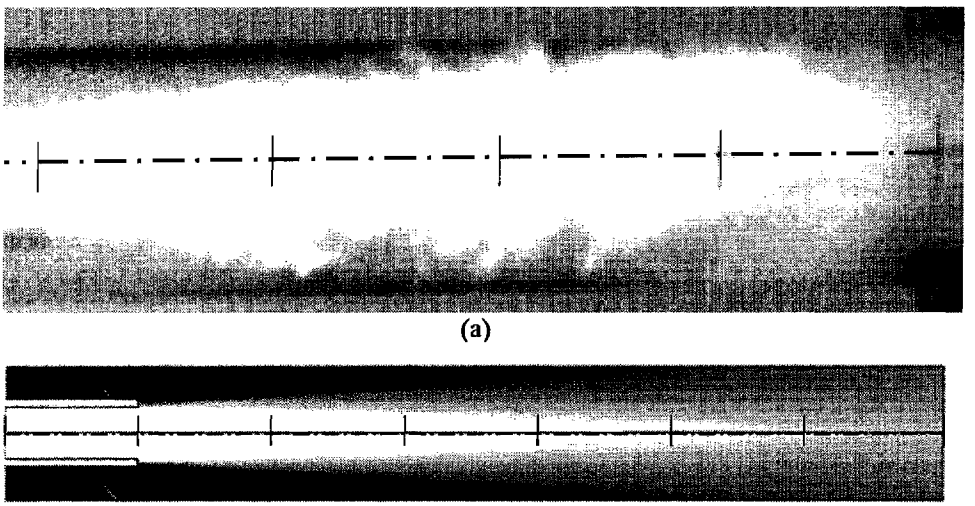

(a)

(b)

Figure 15: Comparisons between the experimental and predicted mixing regions for R_v = 2.89 and c = 0.97%: (a) Representative experimental image and (b) standard k-ε model predictions.

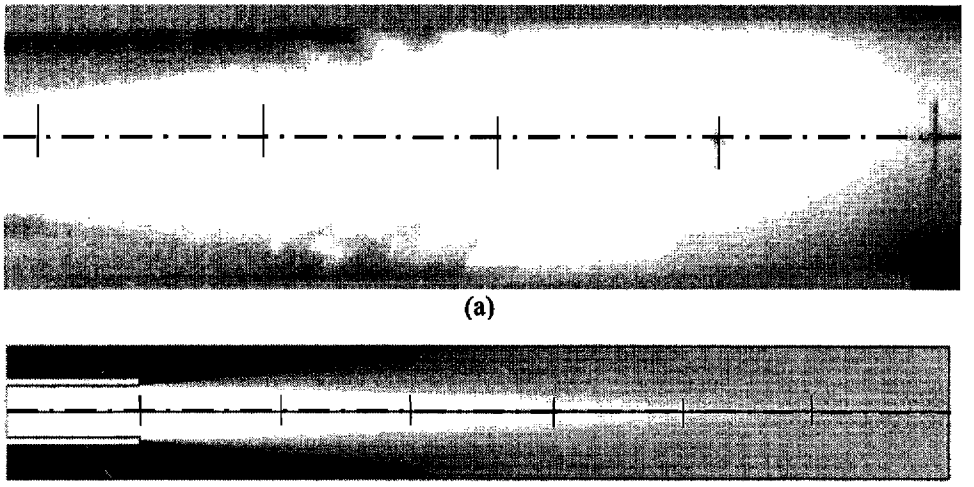

(a)

(b)

Figure 16: Comparisons between the experimental and predicted mixing regions for $R_v = 5.68$ and c = 0.97%: (a) Representative experimental image and (b) standard k-ε model predictions.

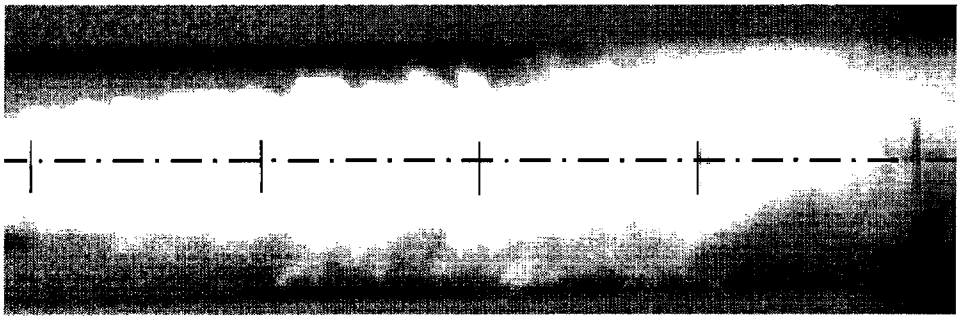

(a)

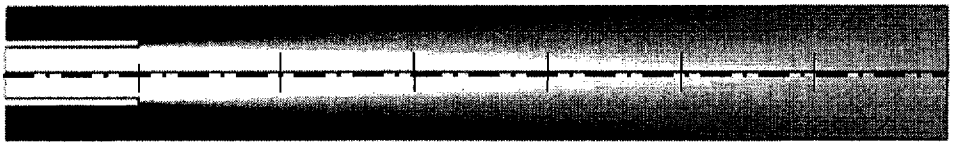

(b)

Figure 17: Comparisons between the experimental and predicted mixing regions for $R_v = 2.95$ and c = 1.86%: (a) Representative experimental image and (b) standard k-ε model predictions.

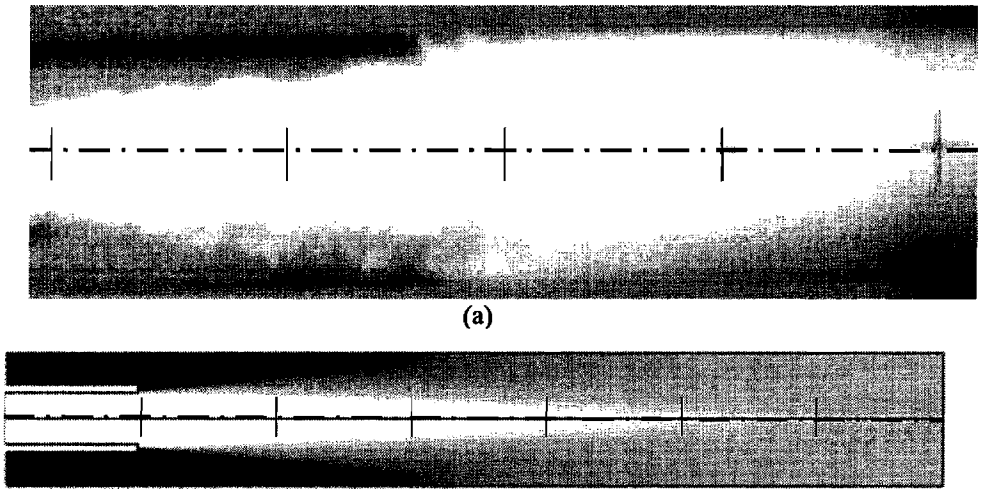

(a)

(b)

Figure 18: Comparisons between the experimental and predicted mixing regions for $R_v = 5.56$ and $c = 1.86\%$: (a) Representative experimental image and (b) standard k-ε model predictions.

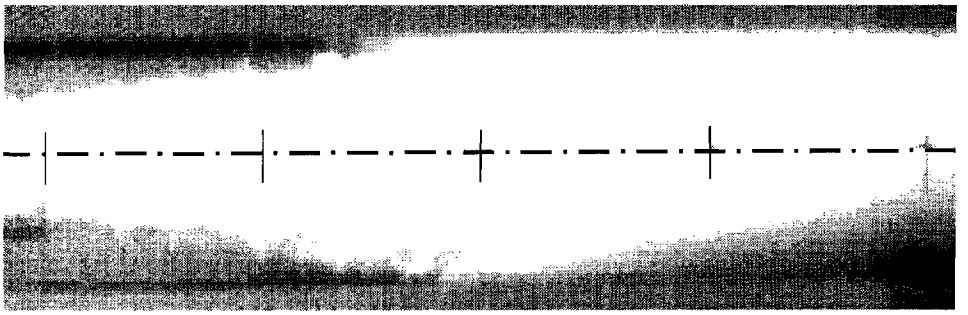

(a)

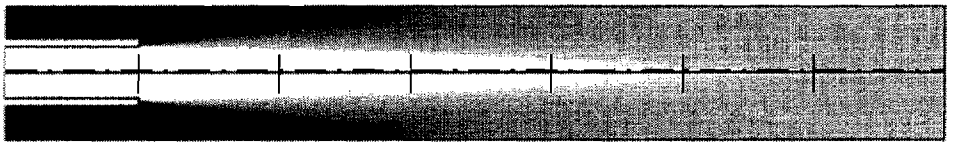

(b)

Figure 19: Comparisons between the experimental and predicted mixing regions for $R_v = 5.92$ and $c = 2.91\%$: (a) Representative experimental image and (b) standard k-ε model predictions.